# Towards Prediction of Non-Radiative Decay Pathways in Organic Compounds I: The Case of Naphthalene Quantum Yields

Alexander W. Kohn,[†,‡] Zhou Lin,[†,‡] and Troy Van Voorhis[*,†]

†*Department of Chemistry, Massachusetts Institute of Technology, Cambridge, MA 02139*

‡*These authors contributed equally.*

E-mail: tvan@mit.edu

**Abstract**

Many emerging technologies depend on human's ability to control and manipulate the excited-state properties of molecular systems. These technologies include fluorescent labeling in biomedical imaging, light harvesting in photovoltaics, and electroluminescence in light-emitting devices. All of these systems suffer from non-radiative loss pathways that dissipate electronic energy as heat, which causes the overall system efficiency to be directly linked to quantum yield ($\Phi$) of the molecular excited state. Unfortunately, $\Phi$ is very difficult to predict from first principles because the description of a slow non-radiative decay mechanism requires an accurate description of long-timescale excited-state quantum dynamics. In the present study, we introduce an efficient semi-empirical method of calculating the fluorescence quantum yield ($\Phi_{\text{fl}}$) for molecular chromophores, which, based on machine learning, converts simple electronic energies computed using time-dependent density functional theory (TDDFT) into an estimate of $\Phi_{\text{fl}}$. As with all machine learning strategies, the algorithm needs to be trained on fluorescent dyes for which $\Phi_{\text{fl}}$'s are known, so as to provide a black-box method which can later predict $\Phi$'s for chemically similar chromophores that have not been studied experimentally. As a first illustration of how our proposed algorithm can be trained, we examine a family of 25 naphthalene derivatives. The simplest application of the energy gap law is found to be inadequate to explain the rates of internal conversion (IC) or intersystem crossing (ISC) – the electronic properties of at least one higher-lying electronic state ($S_n$ or $T_n$) or one far-from-equilibrium geometry are typically needed to obtain accurate results. Indeed, the key descriptors turn out to be the transition state between the Franck–Condon minimum a distorted local minimum near an $S_0/S_1$ conical intersection (which governs IC) and the magnitude of the spin–orbit coupling (which governs ISC). The resulting $\Phi_{\text{fl}}$'s are predicted with reasonable accuracy ($\pm$ 22%), making our approach a promising ingredient for high-throughput screening and rational design of the molecular excited states with desired $\Phi$'s. We thus conclude that our model, while semi-empirical in nature, does in fact extract sound physical insight into the challenge of describing non-radiative relaxations.

# Introduction

The rational design of photophysically and photochemically functional materials requires an understanding of their electronic properties.[1–3] For example, the efficiency of many organic electronic devices depends directly on its fluorescence quantum yield ($\Phi_{\mathrm{fl}}$), defined by the competition between the fluorescence rate ($k_{\mathrm{fl}}$) and the non-radiative rate ($k_{\mathrm{nr}}$):

$$\Phi_{\mathrm{fl}} = \frac{k_{\mathrm{fl}}}{k_{\mathrm{fl}} + k_{\mathrm{nr}}}. \tag{1}$$

The most obvious example of a photophysical technology where $\Phi_{\mathrm{fl}}$ is important is an organic light-emitting diode (OLED), in which the total emission efficiency is directly proportional to $\Phi_{\mathrm{fl}}$: if an exciton formed in the device undergoes rapid non-radiative decay, no photon is emitted.[4] Similarly, for an organic solar cell (OSC) $k_{\mathrm{fl}}$ and $k_{\mathrm{nr}}$ determine the exciton lifetime and thereby the probability that an exciton generates charge carriers.[5] These $k_{\mathrm{nr}}$'s are important in many other fields, including: phosphorescent OLEDs,[6–8] biomedical labeling,[9–11] photodynamic therapy,[12–14] laser dyes,[15–17] and luminescent solar concentrators.[18–20]

In reality, the prediction of quantum yields ($\Phi$) has been very difficult. A complete understanding of $\Phi$ requires a deep understanding of all the relevant non-radiative decay channels. As these decay channels are, by definition, not optically active, they are difficult to study spectroscopically. For a conventional closed-shell organic molecule, common decay pathways to consider include: internal conversion (IC, $S_1 \rightarrow S_0$), intersystem crossing (ISC, $S_1 \rightarrow T_n$), electron removal and addition ($S_1 \rightarrow D^+$, $S_1 \rightarrow A^-$), and photochemical isomerization ($S_1 \rightarrow S_0^*$).[21] It is challenging to address all of these pathways simultaneously, so we narrow the scope in the present study and focus on the most common decay channels in organic compounds – IC and ISC.

Historically, discussion of IC and ISC has been dominated by the energy gap law.[22–24] When the donating state ($S_1$) and the accepting state ($S_0$, $T_n$) are sufficiently well-separated, the Franck–Condon (FC) factor mediating the transfer decay exponentially with the energy

gap between the two levels.[22–24] The energy gap law thus predicts that the logarithm of the IC rate ($k_{\mathrm{IC}}$) is proportional to the fluorescence energy ($E_{\mathrm{fl}}$):

$$k_{\mathrm{IC}} = A \exp\left(-\frac{E_{\mathrm{fl}}}{k_{\mathrm{B}}T}\right). \tag{2}$$

Eq. (2) is widely used in experimental studies.[24–29]

In the past few decades, the energy gap law has been found to be insufficient.[30] Most crucially, the energy gap law and the very idea of Born–Oppenheimer approximation fail at conical intersections (CI), regions in the phase space where electronic potential energy surfaces (PES) meet one another and the interstate coupling becomes infinite. CIs have been found to be ubiquitous in a variety of chemical systems, including biomolecules where the CIs are believed to help protect from the photodamage. At these CIs a coherent transfer can occur on a sub-picosecond timescale, dominating the overall $k_{\mathrm{IC}}$.[31–42]

Computational studies examining IC pathways involving CIs have become more prevalent in the last decade. Unfortunately, IC is a challenging process to model because it arises from non-adiabatic nuclear dynamics.[32,36,37,40,42–47] Earlier studies have proposed two broad categories of approaches to solve the non-adiabaticity problem. The first approach is to explicitly account for nuclear motions with approximate solutions to the electronic structure.[43–45] The most common way to do this is to run a swarm of trajectories on a real electronic PES. However, converging these trajectories can be very expensive, necessitating a large number of trajectories, and thus limiting the throughput of the approach.[36,37,40] The second approach constructs a static PES from several key molecular geometries of the system in question (usually the global/local minimum and the minimum energy conical intersections (MECI) on the CI seam).[32,42,47] The location of a CI is highly sensitive to the quality of the electronic wave function in use, so the cost of the electronic structure method often limits the size of molecule that can be studied here.

Studies of ISC have also advanced substantially in the past decade.[46,48–55] Although ISC

usually dominates the non-radiative dynamics for small molecules (*e.g.*, the triplet quantum yield in naphthalene, $\Phi_{\mathrm{T}} \cong 0.75$[56]), it is a spin-forbidden process that is usually thought not to be responsible for a rapid non-radiative decay, although there are recent counterexamples like 1-nitronaphthalene for which the timescale $\tau_{\mathrm{ISC}} \sim 100$ fs.[48] Compared to IC, ISC is easier to model empirically because it is mediated by spin–orbit coupling (SOC), which can typically be treated perturbatively for organic chromophores. If one works with the spin-diabatic states under the Condon approximation (in which the coupling is independent of nuclear positions), ISC follows a simple rate equation:[57]

$$k_{\mathrm{ISC}} = \frac{2\pi}{\hbar}|H_{\mathrm{SOC}}|^2 \rho(E_{\mathrm{i}} - E_{\mathrm{f}}). \tag{3}$$

The evaluation of $\rho(E_{\mathrm{i}} - E_{\mathrm{f}})$ can still be challenging – the number of FC factors increases dramatically with the number of normal modes.[46] In addition, to quantitatively evaluate $k_{\mathrm{ISC}}$ it is sometimes necessary to go beyond the simple Condon approximation, resulting in a truly *ab initio* calculation being computationally infeasible.[50]

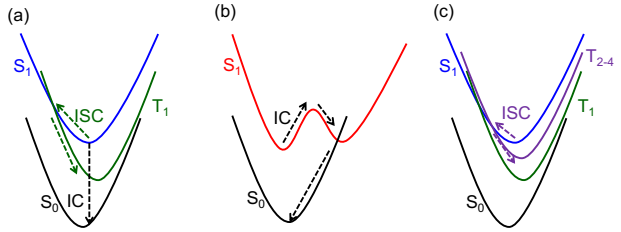


Figure 1: ISC and IC processes investigated in the present study. (a) Direct IC and ISC in which the final states are $S_0$ and $T_1$ respectively. (b) Indirect IC that allows a conformational change of $S_1$ prior to the decay. (c) Indirect ISC in which the final state is a high-lying triplet excited state ($T_{2-4}$).

In the present work we aim to develop a method to understand and predict $\Phi_{\mathrm{fl}}$'s for popular molecular chromophores using only simple and easily accessible information from inexpensive DFT calculations. As should be clear from the discussion above, the DFT calculations themselves do not directly predict $\Phi_{\mathrm{fl}}$ – they are missing key dynamical information required for a first-principles prediction. The key realization, then, is that there is a

large body of molecules for which $\Phi_{\text{fl}}$'s are known experimentally. One can thus use machine learning that is trained on the experimental data to correct for the missing dynamical effects.

As an illustration, in the present study we show how this approach works for the case of a set of naphthalene derivatives. We show how easily computed quantities such as energy gaps, minimum energy conical intersections (MECI), and SOC, can be combined in order to yield quantitative predictions of $\Phi_{\text{fl}}$'s. We discover that, in most cases, information about higher-lying excited states ($S_n$ and $T_n$) are required to obtain any reasonable description of $\Phi_{\text{fl}}$. For example, the 1-aminonaphthalene species are dominated by IC mediated by a transition to a conformation with the amino group distorted out of plane (Fig. 1(b)), which is essentially an $S_1 \rightarrow S_0^*$ isomerization in the adiabatic framework. On the other hand, the alkyl and aryl-substituted naphthalene species are dominated by ISC between $S_1$ and high-lying triplet states $T_{2-4}$ (Fig. 1(c)). Based on our discovery, the simple energy gap law and direct IC and ISC processes (Fig. 1(a)) are not sufficient to explain the variations in either $k_{\text{IC}}$ or $k_{\text{ISC}}$. Using our semi-empirical model, we can reproduce $k_{\text{fl}}$, $k_{\text{IC}}$, and $k_{\text{ISC}}$ with mean absolute errors (MAE) of 0.38, 0.68, and 0.34 decades, respectively, and can predict $\Phi_{\text{fl}}$ with a MAE of 0.22 and a mean signed error (MSE) of 0.10. This study shows how one can understand these ubiquitous decay processes using inexpensive quantum chemical theory.

# Theory

## Test Molecules

In the present study, we focus on the photophysical processes which occur within two sub-families of naphthalene species (Fig. 2): alkyl- and aryl-substituted naphthalenes (Family I) and 1-aminonaphthalene derivatives (Family II). These families were chosen because of the large quantity of high-quality spectroscopic data that exists in literature to calibrate with, which is very important as the method we outline herein is semi-empirical. The experimental data for Family I were obtained from Berlman *et al.*[58] and those for Family II from the studies

performed by Rückert *et al.*,[59] Suzuki *et al.*,[60] and Takehira *et al.*[61]

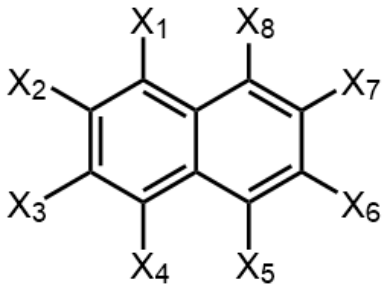


| Family | # | Name | $X_1$ | $X_2$ | $X_3$ | $X_4$ | $X_5$ | $X_6$ | $X_7$ | $X_8$ |
|---|---|---|---|---|---|---|---|---|---|---|
| I[58] | **1** | NAPH | H | H | H | H | H | H | H | H |
| | **2** | 1MN | $CH_3$ | H | H | H | H | H | H | H |
| | **3** | 2MN | H | $CH_3$ | H | H | H | H | H | H |
| | **4** | 1HN | OH | H | H | H | H | H | H | H |
| | **5** | 2HN | H | OH | H | H | H | H | H | H |
| | **6** | 23DMN | H | $CH_3$ | $CH_3$ | H | H | H | H | H |
| | **7** | 26DMN | H | $CH_3$ | H | H | H | $CH_3$ | H | H |
| | **8** | 2PN | H | $C_6H_5$ | H | H | H | H | H | H |
| | **9** | 14DPN | $C_6H_5$ | H | H | $C_6H_5$ | H | H | H | H |
| | **10** | 15DPN | $C_6H_5$ | H | H | H | $C_6H_5$ | H | H | H |
| | **11** | 17DPN | $C_6H_5$ | H | H | H | H | H | $C_6H_5$ | H |
| | **12** | ACN | $C_2H_4$–$X_8$ | H | H | H | H | H | H | $C_2H_4$–$X_1$ |
| II[59–61] | **13** | 1AN | $NH_2$ | H | H | H | H | H | H | H |
| | **14** | 1A4CNN | $NH_2$ | H | H | CN | H | H | H | H |
| | **15** | 1A4CLN | $NH_2$ | H | H | Cl | H | H | H | H |
| | **16** | 1A4MN | $NH_2$ | H | H | $CH_3$ | H | H | H | H |
| | **17** | 1MAN | $NHCH_3$ | H | H | H | H | H | H | H |
| | **18** | 1DMAN | $N(CH_3)_2$ | H | H | H | H | H | H | H |
| | **19** | 1DMA4CNN | $N(CH_3)_2$ | H | H | CN | H | H | H | H |
| | **20** | 1DMA4CLN | $N(CH_3)_2$ | H | H | Cl | H | H | H | H |
| | **21** | 1DMA4MN | $N(CH_3)_2$ | H | H | $CH_3$ | H | H | H | H |
| | **22** | 1DMA4MON | $N(CH_3)_2$ | H | H | $OCH_3$ | H | H | H | H |
| | **23** | 1DMA5MON | $N(CH_3)_2$ | H | H | H | $OCH_3$ | H | H | H |
| | **24** | 1DMA6MON | $N(CH_3)_2$ | H | H | H | H | $OCH_3$ | H | H |
| | **25** | 1DMA7MON | $N(CH_3)_2$ | H | H | H | H | H | $OCH_3$ | H |
| | **26** | 1NAZN | *N*-azetidinyl | H | H | H | H | H | H | H |
| | **27** | 1NPYN | *N*-pyrrolidinyl | H | H | H | H | H | H | H |

Figure 2: Test molecules grouped by appropriate families based on their substituents. Family I (# 1–12) includes alkyl- and aryl-substituted naphthalene species and Family II (# 13–27) consists of 1-aminonaphthalene derivatives.

## Fluorescence Rate

We evaluated $k_{\mathrm{fl}}$ using Einstein's formula for spontaneous emission:[62]

$$k_{\mathrm{fl}} = \frac{4\alpha^3 E_{\mathrm{fl}}^3 |\mu_{\mathrm{fl}}|^2}{3} \tag{4}$$

where $\alpha \simeq 1/137$ represents the fine structure constant, $\mu_{\mathrm{fl}}$ is the fluorescence transition dipole moment (TDM) between $S_1$ and $S_0$. Both $E_{\mathrm{fl}}$ and $\mu_{\mathrm{fl}}$ were calculated using the standard linear-response time-dependent density functional theory (TDDFT) with the Tamm–Dancoff approximation (TDA),[63] at the emissive geometry of $S_1$ which was also optimized using TDDFT. TDA was chosen because of our empirical observation that singlet–triplet instability tends to be common near the MECIs in the excited state, contaminating full TDDFT results. Thus the TDA results, while less rigorous, are more reliable for the quantities we are computing below.

To simplify our investigation we followed Kasha's rule in the present study – all molecules emit from their lowest-energy excited state of a given multiplicity.[64,65] This means that $E_{\mathrm{fl}}$ and $\mu_{\mathrm{fl}}$ become $E_{S_1}$ and $\mu_{S_1}$. To help benchmark our methodology, we also calculated the absorption energy, $E_{\mathrm{abs}}$, based on TDDFT, at the $S_0$ geometry (optimized using ground state DFT).

## Internal Conversion Rate and Conical Intersection

We described $k_{\mathrm{IC}}$ following an Arrhenius-like ansatz modified from Eq. (2),

$$k_{\mathrm{IC}} = A_{\mathrm{IC}} \exp\left(-\frac{E_{\mathrm{a}}}{k_{\mathrm{B}}T}\right). \tag{5}$$

The determinations of the activation energy ($E_{\mathrm{a}}$), and the pre-exponential factor ($A_{\mathrm{IC}}$) were the main tasks of this part of the study.

An earlier CASPT2 study on 1-aminonaphthalene (compound **13**) by Montero *et al.*

showed that CIs play a key role in the photophysics.[66] The complete characterization of a CI between two states is difficult as the CI is in actuality a multi-dimensional hyper-seam.[41] The MECI on this seam is one effective way to describe a CI. To locate the MECI between two PES's, we used the penalty-function method proposed by Levine *et al.*[67] and implemented by Zhang *et al.*[68] (selecting $\gamma = 0.02$ Hartree).

Our principal tool, the standard linear-response TDDFT, does not properly describe a CI as it gives the CI seam an incorrect dimensionality.[69] However, the spin-flip variant of TDDFT (SFDFT)[70] does not have the dimensionality problem and is a useful tool for finding the MECI between $S_1$ and $S_0$ as a rough approximation of the $S_1/S_0$ CI. However, SFDFT necessitates the use of an exotic functional with unusually a large amount of Hartree–Fock (HF) exchange to be accurate:[70–73] we here employed the common BHHLYP (with 50% HF and 50% Becke exchange[74] and the Lee–Yang–Parr correlation[75]).

To anchor our results in the more-familiar linear-response TDDFT approach, we constructed a reaction path from the FC minimum of $S_1$ state to the SFDFT-evaluated MECI geometry using standard linear-response TDDFT and the freezing string method (FSM),[76,77] and located the transition state near the maximum of this reaction path. $E_\mathrm{a}$ in Eq. (5) was calculated as the energy difference between the FC minimum of $S_1$ and the transition state, and $A_\mathrm{IC}$ was obtained from a linear fit between the computed $E_\mathrm{a}$ and the experimental $\log_{10} k_\mathrm{IC}$.

## Intersystem Crossing Rate and Spin–Orbit Coupling

We described $k_\mathrm{ISC}$ following a modified version of Eq. (3),

$$k_\mathrm{ISC} = B_\mathrm{ISC} + C_\mathrm{ISC} \sum_i |H_\mathrm{SOC}^{\mathrm{S_1/T}_i}|^2, \tag{6}$$

in which $H_\mathrm{SOC}^{\mathrm{S_1/T_i}}$ represents the SOC between $S_1$ and energetically-local triplets ($T_i$) and $B_\mathrm{ISC}$ and $C_\mathrm{ISC}$ are fit parameters.

Recent work by Marian and coworkers[78] has expanded the calculation of $H_{\mathrm{SOC}}^{\mathrm{S_1/T}_i}$ within the framework of TDDFT. Herein we employed the one-electron Breit–Pauli Hamiltonian,[79]

$$H_{\mathrm{SOC}} = -\frac{\alpha^2}{2} \sum_{k,A} \frac{Z_A}{r_{kA}^3} (\mathbf{r}_{kA} \times \mathbf{p}_k) \cdot \mathbf{s}_k, \tag{7}$$

and evaluated $H_{\mathrm{SOC}}^{\mathrm{S_1/T}_{i=2-4}}$ at the TDDFT-optimized $S_1$ geometry. In Eq. (7) $k$ and $A$ index electrons and nuclei, $Z_A$ is the charge of nucleus $A$, $\mathbf{p}_k$ and $\mathbf{s}_k$ are the momentum and spin vectors of electron $k$ respectively, and $\mathbf{r}_{kA}$ represents the displacement vector from nucleus $A$ to electron $k$. $B_{\mathrm{ISC}}$ and $C_{\mathrm{ISC}}$ were obtained from the linear fit of the relation between the computed $|H_{\mathrm{SOC}}^{\mathrm{S_1/T}_i}|^2$ and the experimental $k_{\mathrm{ISC}}$.

## Quantum Yield

In the present study, we computed $\Phi_{\mathrm{fl}}$ following Eq. (1) and employed[80]

$$k_{\mathrm{nr}} \simeq k_x \quad (x = \mathrm{IC} \quad \mathrm{or} \quad \mathrm{ISC}). \tag{8}$$

Eq. (8) expresses the assumption that one of the two decay processes, either IC or ISC, is considered dominant (more than one order of magnitude greater than any other non-radiative decay process). Although we chose the dominant pathway based on experimental evidence, we believed that extending our methodology to be fully black-box is viable. In particular, when focusing on only one decay process or the other, we found that simple regression is effective at predicting $k_{\mathrm{nr}}$'s. For a general case, we anticipated that an artificial neural network[81–83] would easily be able to decide which pathway is more likely to dominate and choose the appropriate descriptor.

### Computational Details

All DFT calculations were performed in Q-Chem 4.4[84] using the $\omega$B97X-D3 functional[85] and the 6-31G* basis set,[86] except when explicitly noted. $\omega$B97X-D3 was used because most popular XC functionals like B3LYP struggle to reproduce the $S_1/S_2$ ($L_b/L_a$) ordering in polycyclic aromatic hydrocarbons like naphthalene derivatives.[87,88] For example, for plain naphthalene (compound **1**) B3LYP inverts the $S_1/S_2$ gap ($E(S_2) - E(S_1) = -0.09$ eV) compared to the experimental value (0.53 eV), while $\omega$B97X-D3 predicts the correct ordering with a gap of 0.32 eV.

## Results and Discussion

### Fluorescence Energies and Rates

To compute $\Phi_{\text{fl}}$ of a given molecule we first need an accurate emissive geometry. We employed standard TDDFT/TDA to acquire $S_1$ geometries and reproduced $E_{\text{fl}}$'s with a MAE of 0.71 eV, as shown in Fig. 3(a). The MAE of $E_{\text{abs}}$'s is 0.66 eV, with results presented in Fig. S1 of the Supporting Information (SI). Both results appear quite poor for TDDFT, for which the typical intrinsic MAE is $\sim$0.3 eV. Fig. 3(a) illustrates that this large MAE arises from a uniform overestimation of the predicted $E_{\text{fl}}$'s. Simply calibrating our results by treating 0.71 eV as a systematic error and subtracting it from all $E_{\text{fl}}$'s produced an improved MAE of 0.06 eV, reflecting that our results are qualitatively very accurate.

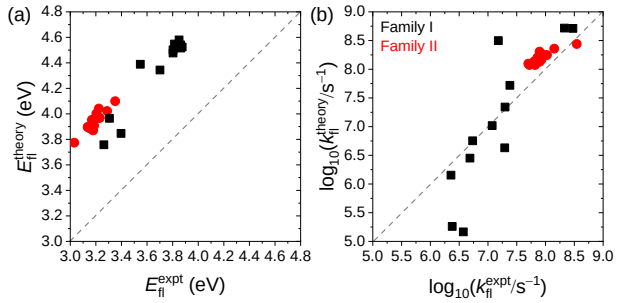


Figure 3: Comparison between the theoretical and experimental values for (a) $E_{\mathrm{fl}}$'s and (b) $k_{\mathrm{fl}}$'s for Kasha emissions ($S_1 \rightarrow S_0$). The dashed lines show perfect predictions. Molecules in Families I and II are represented by black squares and red circles, respectively.

Having obtained satisfactory emissive geometries, we compared calculated $k_{\mathrm{fl}}$'s against the experiments based on Eq. (4) and presented the results in Fig. 3(b). While past studies reported that the TDDFT evaluation of $\mu_{\mathrm{fl}}$ is difficult,[87,88] we found the calculated $\mu_{\mathrm{fl}}$'s acceptable, reproducing $k_{\mathrm{fl}}$'s with a MAE of 0.38 decades. Much of the error arises from large underestimations of $k_{\mathrm{fl}}$'s of the poorly emissive compounds naphthalene (**1**) and 1-methylnaphthalene (**2**), possibly reflecting the limitation of the "frozen" Condon approximation.

## Direct Intersystem Crossing and Internal Conversion Transitions

As discussed in the introduction, conventional models of IC and ISC are often limited to a direct transfer from $S_1$ to $S_0$ and $T_1$, respectively. Under the energy gap law assumption (*e.g.* Eq. (2)), $\log_{10}k_{\mathrm{nr}}$ should be linearly anticorrelated with the energy gap. To evaluate the quality of such an energy gap law relation, we started with direct IC and checked the predictive utility of $E_{\mathrm{fl}}$ and the reorganization energy of direct IC ($\lambda_{\mathrm{IC}}$, Fig. 1(a)), which is defined in Marcus theory[89] and coincides with half of the Stokes shift ($E\mathrm{ss} = E_{\mathrm{abs}} - E_{\mathrm{fl}}$).[90] Fig. 4 (a) and (b) illustrates the reported experimental $k_{\mathrm{nr}}$ as a function of the experimental $E_{\mathrm{fl}}$ and $\lambda_{\mathrm{IC}}$. Here we used experimental photophysical observables as the independent variables in order to show that the problem does not lie in the quality of electronic structure theory, but in the energy gap law model itself. As one can see, both

correlations are poor.

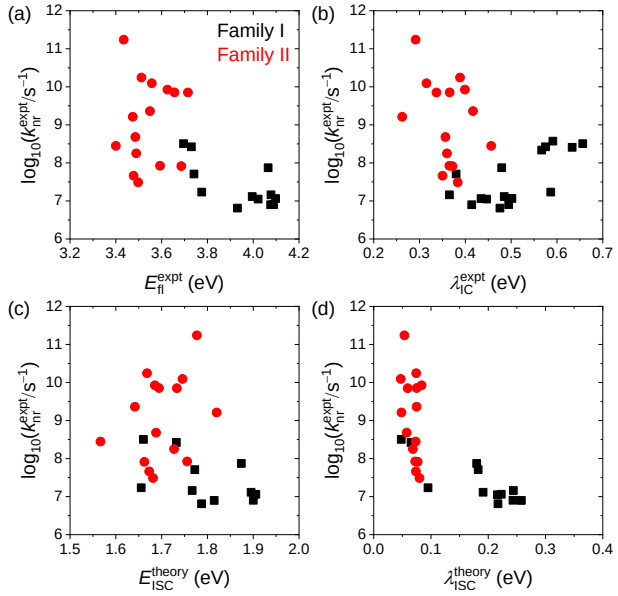


Figure 4: Energy gap law correlations between the experimental $\log_{10}k_{\rm nr}$ and the experimental (a) $E_{\rm fl}$ and (b) $\lambda_{\rm IC}$ for the direct $S_1 \rightarrow S_0$ IC, and between the experimental $\log_{10}k_{\rm nr}$ and the computed adiabatic (c) $E_{\rm ISC}$ and (d) $\lambda_{\rm ISC}$ for the direct $S_1 \rightarrow T_1$ ISC. Molecules in Families I and II are presented by black squares and red circles, respectively.

We performed a similar analysis for direct ISC (Fig. 1(a)), using the computed adiabatic energy gap ($E_{\rm ISC}$) and reorganization energy ($\lambda_{\rm ISC}$) and plotting their correlations with the experimental $\log_{10}k_{\rm nr}$ in Fig. 4 (c) and (d). These results indicate an analogous difficulty predicting $k_{\rm ISC}$ using simply the energy gap law. Overall, our results support the conclusion that the energetics of $S_1$ and $T_1$ are generally insufficient to predict $k_{\rm nr}$'s on their own. As we will see below, $\Phi_{\rm fl}$ typically has a critical dependence on higher-lying electronic states or far-from-equilibrium geometries, which must be accounted for if one expects accurate predictions.

## Intersystem Crossing

We found that $k_{\rm ISC}$'s for the alkyl- and aryl-substituted naphthalene compounds (Family I)[58] are best modeled by Eq. (6). This equation uses a "frozen" Condon approximation,[57] with the additional assumption that all energetically-relevant accepting states ($T_2$, $T_3$, and

$T_4$) have equal accepting densities of states at the energy of the donating $S_1$ state. Herein we plot the experimental $\log_{10}k_{\rm nr}$ versus the computed total $\log_{10}k_{\rm ISC}$ in Fig. 5, showing a reproduction of the experimental $k_{\rm nr}$'s with a MAE of 0.34 decades, which is extremely good. We also experimented with other relations that incorporate energetic dependence into an Arrhenius-like or Marcus-like expression, but at least for this case there is no correlation between the TDDFT energies and $k_{\rm ISC}$'s. The difficulty might originate in the very small $S_1/S_2$ gap for Family I, which challenges the accuracy of our excited-state methodology.

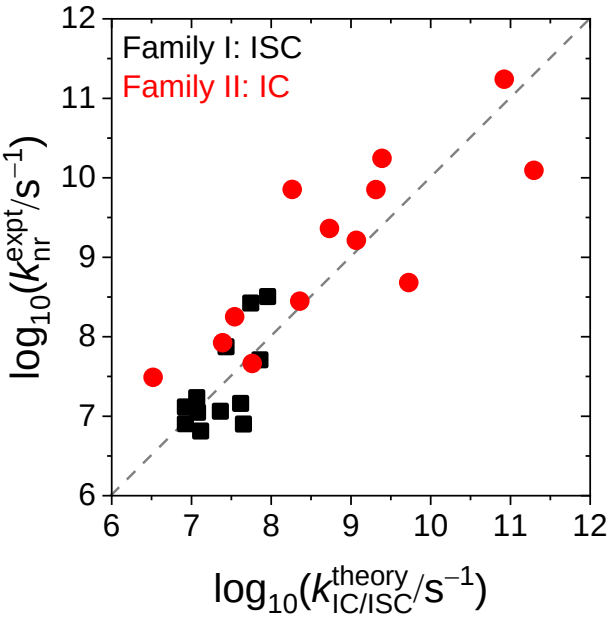


Figure 5: Comparison between the computed $k_{\rm ISC}$ (Family I, black squares) or $k_{\rm IC}$ (Family II, red circles) and the experimental $k_{\rm nr}$ on the logarithm scale. Family I are dominated by IC while Family II are dominated by ISC.

## Internal Conversion

One of the advantages of the 1-aminonaphthalene data set (Family II) is the availability of experimental $E_{\rm a}$'s of IC (Eq. (5)). Fig. 6 shows the experimental $\log_{10}k_{\rm nr}$ versus the experimental $E_{\rm a}$. The results are compared to the TDDFT-evaluated $E_{\rm a}$ required to reach the transition state from the FC minimum along a reaction path similar to the one shown in Fig. 7.

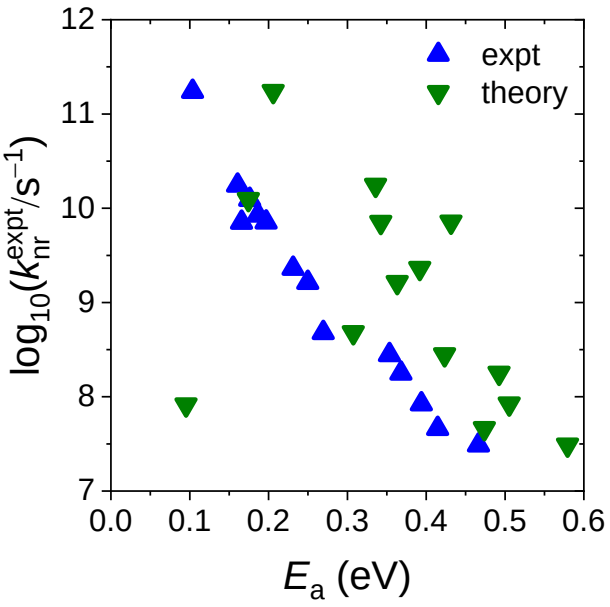


Figure 6: Energy gap law correlations between the experimental $\log_{10}k_{nr}$ and the experimental (blue up triangles) or TDDFT-evaluated (green down triangles) $E_a$ for 1-aminonaphthalene derivatives (Family II).

We observed that the experimental $E_a$ is a very good predictor of the experimental $k_{nr}$ through the modified energy gap law (similar to Eq. (5)) – the prefactor $A$ varies very little. As shown in Fig. 6, although TDDFT slightly overestimates the experimental $E_a$'s it captures the variation of $A$ very well. A simple linear fit of the $\log_{10}k_{nr}$ to the TDDFT-computed $E_a$ allows us to reproduce $k_{nr}$ accurately with a MAE of 0.68 decades (Fig. 5), which is in a fairly good agreement given that these $k_{nr}$'s vary over four decades. Figs. 5 and 6 show that these $E_a$'s predict $k_{IC}$'s very accurately – we have now constructed an adequate method for computing the total $k_{nr}$'s of 1-aminonaphthalenes derivatives. In addition, we can use the SFDFT[70] approach and the BHHLYP functional[74,75] to evaluate the $S_1/S_0$ MECI, and directly construct a Bell–Evans–Polanyi model[91,92] using the theoretical energy gap between the $S_1$ FC minimum and this MECI. The result, presented in Fig. S2 of the SI, reproduces $k_{IC}$ with a MAE of 0.27 decades.

Above, we showed that IC occurring in Family II cannot be understood as a one-step, direct $S_1 \rightarrow S_0$ transition from the vicinity of the emissive geometry. It is thus interesting to evaluate the nature of the transition state involved. The computed reaction path for

1-aminonaphthalene (**13**) is shown in Fig. 7, highlighting the distorted molecular configurations of the MECI and the transition state near it. The resulting structure is characteristic of all members of Family I: IC is mediated by a transition from the FC minimum to a novel conformer with the amino group and the $C_1$ atom (Fig. 2) bonded to it dragged nearly perpendicular to the naphthalene plane. When stretched in this manner, the transition density is localized to the amino group and the $C_1$ and $C_2$ atoms (Fig. 7).

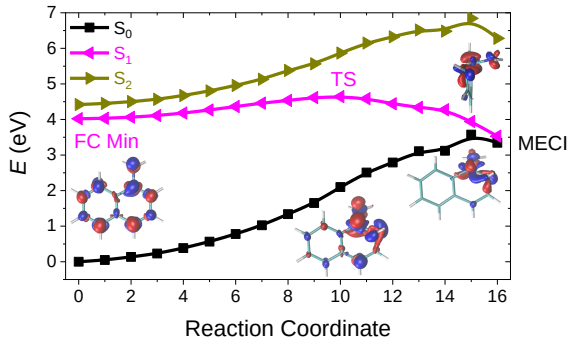


Figure 7: PES's are plotted along the IC reaction coordinate for the $S_0$ (black squares), $S_1$ (magenta left triangles), and $S_2$ (dark yellow right triangles) states of 1-aminonapthalene (compound **13**). From left to right, we present molecular geometries and transition densities for the $S_1$ PES at the FC minimum, the transition state, and at the $S_0/S_1$ MECI (side and front views).

This conformational isomerization mechanism ($S_1 \rightarrow S_0^*$) rationalizes trends observed in the experimental measurements of **13**. For a given amino substitution, a roughly inverse energy gap law relation is observed: as $E_{\mathrm{fl}}$ decreases, $k_{\mathrm{IC}}$ also decreases. This is contrary to the conventional wisdom, but can be easily understood in our framework. If the IC process is simply limited by the activation of a transition state, under a Bell–Evans–Polanyi model we would predict that the relative energies of the two minima provide $E_{\mathrm{a}}$.[91,92] Assuming identical energies of the near-CI region for all species with the same amino substitution (justified by the spatial localization of the excitation near the amino group), $E_{\mathrm{a}}$ is determined only by the energy of the near-FC region, which is conveniently probed by $E_{\mathrm{fl}}$ . A larger $E_{\mathrm{fl}}$ indicates a more downhill IC mechanism, implying a more energetically accessible transition state and thus a faster IC process, in opposition to the traditional energy gap model.

The nature of the IC pathway for compounds in Family II has been investigated in

several past studies.[59–61] Most notably, Montero *et al.*[66] performed CASPT2 calculations and concluded that IC decay proceeded via an $S_1/S_2$ CI followed by transfer through an $S_2/S_0$ CI. However, experimentally they found no evidence for a relevant $S_1/S_2$ CI in the photodynamics. Our results do not necessarily rule out the presence of an $S_1/S_2$ CI or its relevance to IC in these derivatives. However, our comparison over a broad family of derivatives shows that any relevant information about the $S_1/S_2$ CI must be encoded in the transition state – either because going over the transition state is the rate-determining step or because the electronic structures of $S_1$ and $S_2$ are substantially mixed at the transition state. This kind of insight cannot be obtained from a case study on a single derivative.

## Quantum Yield Evaluation

With all of the results obtained above, we can finally evaluate our ability to compute $\Phi_{fl}$ using Eq. (1). We illustrate in Fig. 8 the correlation between our computed $\Phi_{fl}$'s and the experimental values, achieving a MAE of 0.22 and a MSE of 0.10.

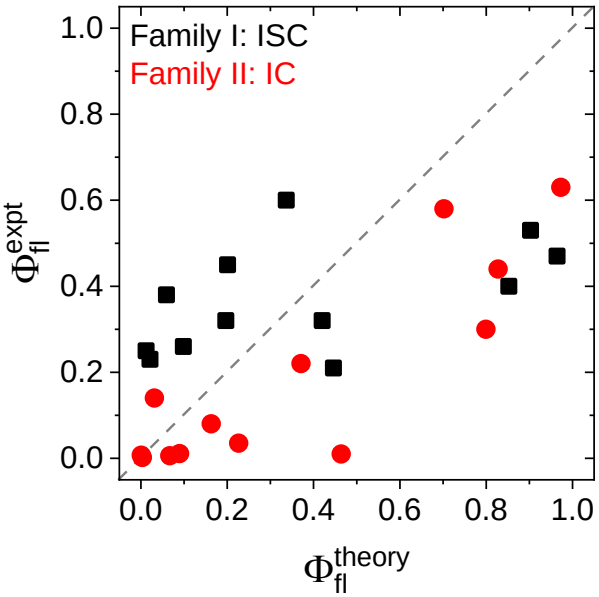


Figure 8: Comparison between computed and the experimental $\Phi_{fl}$'s. Family I are dominated by IC while Family II are dominated by ISC.

We visually note that these plots illustrate one of the challenges in the estimation of

$\Phi_{fl}$: while the predicted $k_{fl}$'s and $k_{nr}$'s are obviously quite good, the resulting $\Phi_{fl}$'s are less inspiring. The reason for this is the non-linear nature of $\Phi_{fl}$: cases with very fast (slow) $k_{nr}$'s are squeezed together near $\Phi_{fl} \approx 0$ ($\Phi_{fl} \approx 1$), leading to a high sensitivity to errors over a small range of $k_{nr}$'s.

We therefore analyzed which predicted components, $k_{fl}$ or $k_{nr}$, limit the accuracy of $\Phi_{fl}$ most by replacing either computed $k_{fl}$ or $k_{nr}$ with its experimental counterpart in Eq. (1). If we combined the computed $k_{fl}$'s with the experimental $k_{nr}$'s, we obtained $\Phi_{fl}$'s with a MAE of 0.12, which is comparable to the experimental error.[58] Similarly, when we combined the computed $k_{IC}$'s of Family II with the experimental $k_{fl}$'s we arrived at a MAE of 0.12 which, again, is very accurate. However, combining the computed $k_{ISC}$'s of Family I with the experimental $k_{fl}$'s produces a MAE of 0.16, slightly worse than the other results. This result suggests that the greatest room for improvement lies in $k_{ISC}$'s, which is unsurprising considering the crudeness of our approximations.

## Conclusions and Future Work

In the present work, we analyzed the components necessary for the calculation of $\Phi_{fl}$, determined from competition between $k_{fl}$ and the relevant $k_{nr}$ for the system. When combined with appropriate training on experimentally known values of $\Phi_{fl}$, we found that TDDFT is an adequate tool to compute the absolute $k_{fl}$, yielding a MAE of 0.38 decades. In particular, our results call into question any attempts to predict $\Phi$'s based on near-equilibrium energetics of the lowest-lying excited states ($S_1$ and $T_1$). In all cases, we discovered that far-from-equilibrium conformations and/or higher-lying excited states play a central role in accurately predicting $\Phi_{fl}$. In particular, heuristics such as the energy gap law seem to provide unreliable conclusions.

Herein, we provided more reliable predictions of $k_{nr}$'s by constructing and using a semi-empirical model for the specific case of napthalene derivatives. For IC-dominated species

we introduced an Arrhenius-like scheme using the TDDFT-evaluated $E_a$ for the transition from the FC minimum of the $S_1$ PES to a novel, amino-distorted transition-state conformer reproducing $k_{IC}$'s with a MAE of 0.68 decades. For ISC-dominated ones we applied a "frozen" Condon approximation in which $T_2$, $T_3$, and $T_4$ are all equally accessible, resulting in $k_{ISC}$'s with a MAE of 0.34 decades. Combining these results, we obtained $\Phi_{fl}$'s with a MAE of 0.22 and a MSE of 0.10.

While the details of the approximations here are not universally applicable (including the frozen Condon approximation and the neglect of the $S_0 \rightarrow S_2$ excitation), we expect that moving forward this study can provide a blueprint for predicting the $\Phi_{fl}$'s of other families of fluorescent dyes. Such studies provide the tantalizing possibility of high-throughput screening of photoactive molecules based on $\Phi$'s: one defines a family of molecules, trains the predictions on a small, representative set of chromophores from that family using a data-driven algorithm like machine learning, and then uses inexpensive computational schemes to screen for potential high-$\Phi_{fl}$ or low-$\Phi_{fl}$ molecules (depending on the demand) within the nearby chemical space that can be synthesized. As the first step in this direction, we anticipate future work on families of molecules for which understanding the photophysical decay pathways are more chemically significant, such as the boron-dipyrromethene (BODIPY) derivatives. More work into understanding ISC pathways in general is also merited, as our understanding evinced here can be improved.

# Acknowledgments

This work was funded by a grant from the United States Department of Energy, Office of Basic Energy Sciences (DE-FG02-07ER46474). We also thank Dr. James Shepherd for insightful and inspirational discussions during the accomplishment of this project.

# References


(1) Anthony, J. E. Functionalized acenes and heteroacenes for organic electronics. *Chem. Rev.* **2006**, *106*, 5028–5048.

(2) Bendikov, M.; Wudl, F.; Perepichka, D. F. Tetrathiafulvalenes, oligoacenenes, and their buckminsterfullerene derivatives: The brick and mortar of organic electronics. *Chem. Rev.* **2004**, *104*, 4891–4945.

(3) Anthony, J. E.; Facchetti, A.; Heeney, M.; Marder, S. R.; Zhan, X. n-Type organic semiconductors in organic electronics. *Adv. Mater.* **2010**, *22*, 3876–3892.

(4) Forrest, S. R.; Bradley, D. D. C.; Thompson, M. E. Measuring the efficiency of organic light-emitting devices. *Adv. Mater.* **2003**, *15*, 1043–1048.

(5) Servaites, J. D.; Ratner, M. A.; Marks, T. J. Practical efficiency limits in organic photovoltaic cells: Functional dependence of fill factor and external quantum efficiency. *App. Phys. Lett.* **2009**, *95*, 2009–2011.

(6) Brown, A. R.; Pichler, K.; Greenham, N. C.; Bradley, D. D. C.; Friend, R. H.; Holmes, A. B. Optical spectroscopy of triplet excitons and charged excitations in poly(p-phenylenevinylene) light-emitting diodes. *Chem. Phys. Lett.* **1993**, *210*, 61 – 66.

(7) Yang, X.; Neher, D.; Hertel, D.; Däubler, T. Highly Efficient Single-Layer Polymer Electrophosphorescent Devices. *Adv. Mater.* **2004**, *16*, 161–166.

(8) Hu, J.-Y.; Ning, Y.; Meng, Y.-S.; Zhang, J.; Wu, Z.-Y.; Gao, S.; Zhang, J.-L. Highly near-IR-emissive ytterbium(III) complexes with unprecendented quantum yields. *Chem. Sci.* **2017**, *8*, 2702–2709.

(9) Zhang, J.; Campbell, R. E.; Ting, A. Y.; Ting, A. Y.; Tsien, R. Y. Creating new fluorescent probes for cell biology. *Nat. Rev. Mol. Cell Biol.* **2002**, *3*, 906–918.

(10) Naumov, P.; Ozawa, Y.; Ohkubo, K.; Fukuzumi, S. Structure and spectroscopy of oxyluciferin, the light emitter of the firefly bioluminescence. *J. Am. Chem. Soc.* **2009**, *131*, 11590–11605.

(11) Vendrell, M.; Zhai, D.; Er, J. C.; Chang, Y. T. Combinatorial strategies in fluorescent probe development. *Chem. Rev.* **2012**, *112*, 4391–4420.

(12) Pineiro, M.; Pereira, M. M.; d'A Rocha Gonsalves, A. M.; Arnaut, L. G.; ao J Formosinho, S. Singlet oxygen quantum yields from halogenated chlorins: potential new photodynamic therapy agents. *J. Photochem. Photobiol. A* **2001**, *138*, 147–157.

(13) Momeni, M. R.; Brown, A. A local CC2 and TDA-DFT double hybrid study on BODIPY/aza-BODIPY dimers as heavy atom free triplet photosensitizers for photodynamic therapy applications. *J. Phys. Chem. A* **2016**, *120*, 2550–2560.

(14) Zou, J.; Yin, Z.; Wang, P.; Chen, D.; Shao, J.; Zhang, Q.; Sun, L.; Huang, W.; Dong, X. Photosensitizer synergistic effects: D–A–D structured organic molecule with enhanced fluorescence and singlet oxygen quantum yield for photodynamic therapy. *Chem. Sci.* **2018**, *9*, 2188–2194.

(15) Jones II, G.; Jackson, W. R.; Halpern, A. M. medium effects on fluorescence quantum yields and lifetimes for coumarin laser-dyes. *Chem. Phys. Lett.* **1980**, *72*, 391–395.

(16) Kubin, R. F.; Fletcher, A. N. Fluorescence quantum yields of some rhodamine dyes. *J. Lumin.* **1982**, *27*, 455–462.

(17) Rurack, K.; Spieles, M. Fluorescence Quantum Yields of a Series of Red and Near-Infrared Dyes Emitting at 600–1000 nm. *Anal. Chem.* **2011**, *83*, 1232–1242.

(18) Currie, M. J.; Mapel, J. K.; Heidel, T. D.; Goffri, S.; Baldo, M. A. High-Efficiency Organic Solar Concentrators for Photovoltaics. *Science* **2008**, *321*, 226–228.

(19) Coropceanu, I.; Bawendi, M. G. Core/Shell Quantum Dot Based Luminescent Solar Concentrators with Reduced Reabsorption and Enhanced Efficiency. *Nano Lett.* **2014**, *14*, 4097–4101.

(20) Meinardi, F.; Colombo, A.; Velizhanin, K. A.; Simonutti, R.; Lorenzon, M.; Beverina, L.; Viswanatha, R.; Klimov, V. I.; Brovelli, S. Large-area luminescent solar concentrators based on 'Stokes-shift-engineered' nanocrystals in a mass-polymerized PMMA matrix. *Nat. Photonics* **2014**, *8*, 392.

(21) Turro, N. J. *Modern Molecular Photochemistry*, 1st ed.; University Science Books, 1991.

(22) Englman, R.; Jortner, J. The energy gap law for radiationless transitions in large molecules. *Mol. Phys.* **1970**, *18*, 145–164.

(23) Caspar, J. V.; Meyer, T. J. Application of the energy gap law to nonradiative, excited-state decay. *J. Phys. Chem.* **1983**, *87*, 952–957.

(24) Chynwat, V.; Frank, H. A. The application of the energy gap law to the $S_1$ energies and dynamics of carotenoids. *Chem. Phys.* **1995**, *194*, 237–244.

(25) Gosztola, D.; Niemczyk, M. P.; Svec, W.; Lukas, A. S.; Wasielewski, M. R. Excited doublet states of electrochemically generated aromatic imide and diimide radical anions. *J. Phys. Chem. A* **2000**, *104*, 6545–6551.

(26) Ulrich, G.; Ziessel, R.; Harriman, A. The chemistry of fluorescent BODIPY dyes: Versatility unsurpassed. *Angew. Chem. Int. Ed.* **2008**, *47*, 1184–1201.

(27) Bullock, J. E.; Vagnini, M. T.; Ramanan, C.; Co, D. T.; Wilson, T. M.; Dicke, J. W.; Marks, T. J.; Wasielewski, M. R. Photophysics and redox properties of rylene imide and diimide dyes alkylated ortho to the imide groups. *J. Phys. Chem. B* **2010**, *114*, 1794–1802.

(28) Duran-Sampedro, G.; Agarrabeitia, A. R.; Garcia-Moreno, I.; Costela, A.; Bañuelos, J.; Arbeloa, T.; López Arbeloa, I.; Chiara, J. L.; Ortiz, M. J. Chlorinated BODIPYs: Surprisingly efficient and highly photostable laser dyes. *Eur. J. Org. Chem.* **2012**, 6335–6350.

(29) Esnal, I.; Urías-Benavides, A.; Gõmez-Durán, C. F. A.; Osorio-Martínez, C. A.; García-Moreno, I.; Costela, A.; Bañuelos, J.; Epelde, N.; Lõpez Arbeloa, I.; Hu, R. et al. Reaction of amines with 8-methylthioBODIPY: Dramatic optical and laser response to amine substitution. *Chem. Asian J.* **2013**, *8*, 2691–2700.

(30) Levine, B. G.; Martínez, T. J. Isomerization through conical intersections. *Annu. Rev. Phys. Chem.* **2007**, *58*, 613–634.

(31) Yarkony, D. R. Conical Intersections: The New Conventional Wisdom. *J. Phys. Chem. A* **2001**, *105*, 6277–6293.

(32) Ismail, N.; Blancafort, L.; Olivucci, M.; Kohler, B.; Robb, M. A. Ultrafast decay of electronically excited singlet cytosine via a $\pi$,$\pi^*$ to $n_O$,$\pi^*$ state switch. *J. Am. Chem. Soc.* **2002**, *124*, 6818–6819.

(33) Yamazaki, S.; Kato, S. Solvent effect on conical intersections in excited-state 9H-adenine: Radiationless decay mechanism in polar solvent. *J. Am. Chem. Soc.* **2007**, *129*, 2901–2909.

(34) Polyakov, I. V.; Grigorenko, B. L.; Epifanovsky, E. M.; Krylov, A. I.; Nemukhin, A. V. Potential energy landscape of the electronic states of the GFP chromophore in different protonation forms: Electronic transition energies and conical intersections. *J. Chem. Theory Comput.* **2010**, *6*, 2377–2387.

(35) Montero, R.; Conde, Á. P.; Ovejas, V.; Castaño, F.; Longarte, A. Ultrafast Photophysics of the Isolated Indole Molecule. *J. Phys. Chem. A* **2012**, *116*, 2698–2703.

(36) Ruckenbauer, M.; Barbatti, M.; Müller, T.; Lischka, H. Nonadiabatic photodynamics of a retinal model in polar and nonpolar environment. *J. Phys. Chem. A* **2013**, *117*, 2790–2799.

(37) Plasser, F.; Crespo-Otero, R.; Pederzoli, M.; Pittner, J.; Lischka, H.; Barbatti, M. Surface hopping dynamics with correlated single-reference methods: 9H-adenine as a case study. *J. Chem. Theory Comput.* **2014**, *10*, 1395–1405.

(38) Giussani, A.; Merchán, M.; Gobbo, J. P.; Borin, A. C. Relaxation mechanisms of 5-azacytosine. *J. Chem. Theory Comput.* **2014**, *10*, 3915–3924.

(39) Nakayama, A.; Yamazaki, S.; Taketsugu, T. Quantum chemical investigations on the nonradiative deactivation pathways of cytosine derivatives. *J. Phys. Chem. A* **2014**, *118*, 9429–9437.

(40) Martínez-Fernández, L.; Corral, I.; Granucci, G.; Persico, M. Competing ultrafast intersystem crossing and internal conversion: a time resolved picture for the deactivation of 6-thioguanine. *Chem. Soc.* **2014**, *5*, 1336–1347.

(41) Xie, C.; Malbon, C. L.; Yarkony, D. R.; Guo, H. Dynamic mapping of conical intersection seams: A general method for incorporating the geometric phase in adiabatic dynamics in polyatomic systems. *J. Chem. Phys.* **2017**, *147*, 044109.

(42) Zhou, Z.; Zhou, X.; Wang, X.; Jiang, B.; Li, Y.; Chen, J.; Xu, J. Ultrafast excited-state dynamics of cytosine aza-derivative and analogues. *J. Phys. Chem. A* **2017**, *121*, 2780–2789.

(43) Chernyak, V.; Mukamel, S. Density-matrix representation of nonadiabatic couplings in time-dependent density functional (TDDFT) theories. *J. Chem. Phys.* **2000**, *112*, 3572–3579.

(44) Baer, R. Non-adiabatic couplings by time-dependent density functional theory. *Chem. Phys. Lett.* **2002**, *364*, 75–79.

(45) Niu, Y.; Peng, Q.; Deng, C.; Gao, X.; Shuai, Z. Theory of excited state decays and optical spectra: Application to polyatomic molecules. *J. Phys. Chem. A* **2010**, *114*, 7817–7831.

(46) Marian, C. M. Spin-orbit coupling and intersystem crossing in molecules. *Wiley Interdiscip. Rev. Comput. Mol. Sci.* **2012**, *2*, 187–203.

(47) Sølling, T. I.; Kuhlman, T. S.; Stephansen, A. B.; Klein, L. B.; Møller, K. B. The Non-Ergodic Nature of Internal Conversion. *ChemPhysChem* **2014**, *15*, 249–259.

(48) Zugazagoitia, J. S.; Almora-Díaz, C. X.; Peon, J. Ultrafast intersystem crossing in 1-nitronaphthalene. An experimental and computational study. *J. Phys. Chem. A* **2008**, *112*, 358–365.

(49) Brédas, J.-L.; Norton, J. E.; Cornil, J.; Coropceanu, V. Molecular Understanding of Organic Solar Cells: The Challenges. *Accounts of Chemical Research* **2009**, *42*, 1691–1699.

(50) Peng, Q.; Niu, Y.; Deng, C.; Shuai, Z. Vibration correlation function formalism of radiative and non-radiative rates for complex molecules. *Chem. Phys.* **2010**, *370*, 215–222.

(51) Endo, A.; Sato, K.; Yoshimura, K.; Kai, T.; Kawada, A.; Miyazaki, H.; Adachi, C. Efficient up-conversion of triplet excitons into a singlet state and its application for organic light emitting diodes. *App. Phys. Lett.* **2011**, *98*, 083302.

(52) Sato, K.; Shizu, K.; Yoshimura, K.; Kawada, A.; Miyazaki, H.; Adachi, C. Organic Luminescent Molecule with Energetically Equivalent Singlet and Triplet Excited States for Organic Light-Emitting Diodes. *Phys. Rev. Lett.* **2013**, *110*, 247401.

(53) An, Z.; Zheng, C.; Tao, Y.; Chen, R.; Shi, H.; Chen, T.; Wang, Z.; Li, H.; Deng, R.; Liu, X. et al. Stabilizing triplet excited states for ultralong organic phosphorescence. *Nat. Mater.* **2015**, *14*, 685.

(54) Gibson, J.; Monkman, A. P.; Penfold, T. J. The Importance of Vibronic Coupling for Efficient Reverse Intersystem Crossing in Thermally Activated Delayed Fluorescence Molecules. *ChemPhysChem* **2016**, *17*, 2956–2961.

(55) Samanta, P. K.; Kim, D.; Coropceanu, V.; Brédas, J.-L. Up-Conversion Intersystem Crossing Rates in Organic Emitters for Thermally Activated Delayed Fluorescence: Impact of the Nature of Singlet vs Triplet Excited States. *J. Am. Chem. Soc.* **2017**, *139*, 4042–4051.

(56) Amand, B.; Bensasson, R. Determination of triplet quantum yields by laser flash absorption spectroscopy. *Phys. Lett.* **1975**, *34*, 44–48.

(57) Nitzan, A. *Chemical dynamics in condensed phases: relaxation, transfer and reactions in condensed molecular systems*; Oxford university press, 2006.

(58) Berlman, I. B. In *Handbook of Fluorescence Spectra of Aromatic Molecules*, 2nd ed.; Berlman, I. B., Ed.; Academic Press, 1971; pp 107–415.

(59) Rückert, I.; Demeter, A.; Morawski, O.; Kühnle, W.; Tauer, E.; Zachariasse, K. A. Internal conversion in 1-aminonaphthalenes. Influence of amino twist angle. *J. Phys. Chem. A* **1999**, *103*, 1958–1966.

(60) Suzuki, K.; Demeter, A.; Kühnle, W.; Tauer, E.; Zachariasse, K. A.; Tobita, S.; Shizuka, H. Internal conversion in 4-substituted 1-naphthylamines. Influence of the electron donor/acceptor substituent character. *Phys. Chem. Chem. Phys.* **2000**, *2*, 981–991.

(61) Takehira, K.; Suzuki, K.; Hiratsuka, H.; Tobita, S. Fast internal conversion in 1-

(dimethylamino)naphthalene: Effects of methoxy substitution on the naphthalene ring. *Chem. Phys. Lett.* **2005**, *413*, 52–58.

(62) van Driel, A. F.; Allan, G.; Delerue, C.; Lodahl, P.; Vos, W. L.; Vanmaekelbergh, D. Frequency-dependent spontaneous emission rate from CdSe and CdTe nanocrystals: Influence of dark states. *Phys. Rev. Lett.* **2005**, *95*, 236804.

(63) Hirata, S.; Head-Gordon, M. Time-dependent density functional theory within the Tamm–Dancoff approximation. *Chem. Phys. Lett.* **1999**, *314*, 291–299.

(64) Soret, J.-L. Analyse spectrale: Sur le spectre d'absorption du sang dans la partie violette et ultra-violette. *Comptes rendus de l'Académie des sciences* **1883**, *97*, 1269–1273.

(65) Kasha, M. Characterization of electronic transitions in complex molecules. *Discuss. Faraday Soc.* **1950**, *9*, 14–19.

(66) Montero, R.; Longarte, A.; Conde, A. P.; Redondo, C.; Castaòno, F.; González-Ramírez, I.; Giussani, A.; Serrano-Andrés, L.; Merchán, M. Photophysics of 1-aminonaphthalene: A theoretical and time-resolved experimental study. *J. Phys. Chem. A* **2009**, *113*, 13509–13518.

(67) Levine, B. G.; Coe, J. D.; Martínez, T. J. Optimizing conical intersections without derivative coupling vectors: Application to multistate multireference second-order perturbation theory (MS-CASPT2). *J. Phys. Chem. B* **2008**, *112*, 405–413.

(68) Zhang, X.; Herbert, J. M. Excited-state deactivation pathways in uracil versus hydrated uracil: Solvatochromatic shift in the $1n\pi^*$ state is the key. *J. Phys. Chem. B* **2014**, *118*, 7806–7817.

(69) Levine, B. G.; Ko, C.; Quenneville, J.; Martínez, T. J. Conical intersections and double excitations in time-dependent density functional theory. *Mol. Phys.* **2006**, *104*, 1039–1051.

(70) Shao, Y.; Head-Gordon, M.; Krylov, A. I. The spin-flip approach within time-dependent density functional theory: Theory and applications to diradicals. *J. Chem. Phys.* **2003**, *118*, 4807–4818.

(71) Huix-Rotllant, M.; Natarajan, B.; Ipatov, A.; Muhavini Wawire, C.; Deutsch, T.; Casida, M. E. Assessment of noncollinear spin-flip Tamm–Dancoff approximation time-dependent density-functional theory for the photochemical ring-opening of oxirane. *Phys. Chem. Chem. Phys.* **2010**, *12*, 12811–12825.

(72) Minezawa, N.; Gordon, M. S. Optimizing conical intersections of solvated molecules: The combined spin-flip density functional theory/effective fragment potential method. *J. Chem. Phys.* **2012**, *137*, 034116.

(73) Herbert, J. M.; Zhang, X.; Morrison, A. F.; Liu, J. Beyond Time-Dependent Density Functional Theory Using Only Single Excitations: Methods for Computational Studies of Excited States in Complex Systems. *Acc. Chem. Res.* **2016**, *49*, 931–941.

(74) Becke, A. D. Density-functional exchange-energy approximation with correct asymptotic behavior. *Phys. Rev. A* **1988**, *38*, 3098–3100.

(75) Lee, C.; Yang, W.; Parr, R. G. Development of the Colle–Salvetti correlation-energy formula into a functional of the electron density. *Phys. Rev. B* **1988**, *37*, 785–789.

(76) Behn, A.; Zimmerman, P. M.; Bell, A. T.; Head-Gordon, M. Efficient exploration of reaction paths via a freezing string method. *J. Chem. Phys.* **2011**, *135*, 224108.

(77) Mallikarjun Sharada, S.; Zimmerman, P. M.; Bell, A. T.; Head-Gordon, M. Automated transition state searches without evaluating the Hessian. *J. Chem. Theory Comput.* **2012**, *8*, 5166–5174.

(78) Dinkelbach, F.; Kleinschmidt, M.; Marian, C. M. Assessment of interstate spin–orbit

couplings from linear response amplitudes. *J. Chem. Theory Comput.* **2017**, *13*, 749–766.

(79) Bethe, H. A.; Salpeter, E. E. *Quantum Mechanics of One- and Two-Electron Atoms*; Plenum Publishing Corporation, New York, 1977; pp 118–204.

(80) Braslavsky, S. E. Glossary of terms used in photochemistry, 3rd edition (IUPAC Recommendations 2006). *Pure Appl. Chem.* **2007**, *79*, 293–465.

(81) Hopfield, J. J.; Tank, D. W. Computing with neural circuits: A model. *Science* **1986**, *233*, 625–633.

(82) Gasteiger, J.; Zupan, J. Neural Networks in Chemistry. *Angew. Chem. Int. Ed.* **1993**, *32*, 503–527.

(83) Wei, J. N.; Duvenaud, D.; Aspuru-Guzik, A. Neural Networks for the Prediction of Organic Chemistry Reactions. *ACS Cent. Sci.* **2016**, *2*, 725–732.

(84) Shao, Y.; Gan, Z.; Epifanovsky, E.; Gilbert, A. T. B.; Wormit, M.; Kussmann, J.; Lange, A. W.; Behn, A.; Deng, J.; Feng, X. et al. Advances in molecular quantum chemistry contained in the Q-Chem 4 program package. *Mol. Phys.* **2015**, *113*, 184–215.

(85) Lin, Y.-S.; Li, G.-D.; Mao, S.-P.; Chai, J.-D. Long-range corrected hybrid density functionals with improved dispersion dorrections. *J. Chem. Theory Comput.* **2013**, *9*, 263–272.

(86) Ditchfield, R.; Hehre, W. J.; Pople, J. A. Self-consistent molecular-orbital methods. IX. An extended Gaussian-type basis for molecular-orbital studies of organic molecules. *J. Chem. Phys.* **1971**, *54*, 724–728.

(87) Grimme, S.; Parac, M. Substantial errors from time-dependent density functional theory

for the calculation of excited states of large $\pi$ systems. *ChemPhysChem* **2003**, *4*, 292–295.

(88) Prlj, A.; Sandoval-Salinas, M. E.; Casanova, D.; Jacquemin, D.; Corminboeuf, C. Low-lying $\pi\pi^*$ states of heteroaromatic molecules: A challenge for excited state methods. *J. Chem. Theory Comput.* **2016**, *12*, 2652–2660.

(89) Marcus, R. A. On the Theory of Oxidation-Reduction Reactions Involving Electron Transfer. I. *J. Chem. Phys.* **1956**, *24*, 966–978.

(90) Lakowicz, J. R. *Principles of Fluorescence Spectroscopy*, 3rd ed.; Springer-Verlag US, 2011.

(91) Bell, R. P. The theory of reactions involving proton transfers. *Proc. Royal Soc. A* **1936**, *154*, 414–429.

(92) Evans, M. G.; Polanyi, M. Further considerations on the thermodynamics of chemical equilibria and reaction rates. *Trans. Faraday Soc.* **1936**, *32*, 1333–1360.

# Graphical TOC Entry

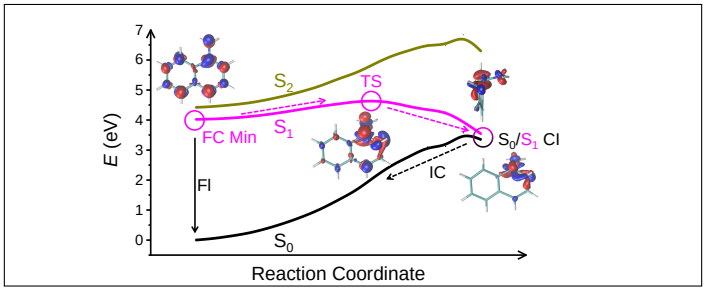

# Supporting Information: Toward Prediction of Non-Radiative Decay Pathways in Organic Compounds I: The Case of Naphthalene Quantum Yields

Alexander W. Kohn,[†,‡] Zhou Lin,[†,‡] and Troy Van Voorhis[*,†]

†*Department of Chemistry, Massachusetts Institute of Technology, Cambridge, MA 02139*

‡*These authors contributed equally.*

E-mail: tvan@mit.edu

CONTENTS:


1. Table S1: Absorption energies ($E_{\mathrm{abs}}$), fluorescent energies ($E_{\mathrm{fl}}$) and radiative rates ($k_{\mathrm{fl}}$) for Family I from theory and experiments.

2. Table S2: Absorption energies ($E_{\mathrm{abs}}$), fluorescent energies ($E_{\mathrm{fl}}$) and radiative rates ($k_{\mathrm{fl}}$) for Family II from theory and experiments.

3. Table S3: Experimental non-radiative rates ($k_{\mathrm{nr}}$) are compared against theoretical direct intersystem crossing (ISC) rates ($k_{\mathrm{ISC}}$) for Family I. Theoretical values of adiabatic energy gaps ($E_{\mathrm{ISC}}$), reorganization energies ($\lambda_{\mathrm{ISC}}$), and Marcus-like activation energies ($E^{\ddagger}_{\mathrm{ISC}}$) are also provided.

4. Table S4: Experimental non-radiative rates ($k_{\mathrm{nr}}$) are compared against theoretical direct internal conversion (IC) rates ($k_{\mathrm{IC}}$) for Family II. Theoretical values of fluorescence energies ($E_{\mathrm{fl}}$), reorganization energies ($\lambda_{\mathrm{IC}}$, half of Stokes shift), and Marcus-like activation energies ($E^{\ddagger}_{\mathrm{IC}}$) are also provided.

5. Figure S1: Comparison between the theoretical and experimental values for absorption energies ($E_{\mathrm{abs}}$) for Families I and II.

6. Figure S2: Energy gap law correlations between the total non-radiative rates ($k_{\mathrm{nr}}$) and the activation energies evaluated using the SFDFT/BHHLYP approach. The activation energy is treated as the difference between the Frank–Condon minimum on the $S_1$ surface and the $S_1/S_0$ minimum energy conical intersection (MECI).

7. Figure S3: The squared transition dipole moments (TDM) for the $S_0 \rightarrow S_1$ and $S_0 \rightarrow S_2$ transitions along the reaction path described in Fig. 6 of the main text. $S_1$ and $S_2$ do not seem to switch in character.

8. Figure S4: The percentage of the largest natural transition orbitals (NTO) of the $S_0 \rightarrow S_1$ and $S_0 \rightarrow S_2$ transitions along the reaction path described in Fig. 6 of the main text. $S_1$ and $S_2$ do not seem to switch in character.

**Table S1: $E_{\mathrm{abs}}$'s, $E_{\mathrm{fl}}$'s and $k_{\mathrm{fl}}$'s for Family I from theory and experiments.**

| | | $E_{\mathrm{abs}}$ (eV) | | $E_{\mathrm{fl}}$ (eV) | | $\log_{10}(k_{\mathrm{fl}}/\mathrm{s}^{-1})$ | |
|---|---|---|---|---|---|---|---|
| # | species | theory | expt[a] | theory | expt[a] | theory[f] | expt[a] |
| **1** | NAPH | 4.66 | 4.31 | 4.27 | 3.85 | 7.97 | 6.38 |
| **2** | 1MN | 4.62 | 4.39 | 4.18 | 3.81 | 8.06 | 6.57 |
| **3** | 2MN | 4.58 | 4.31 | 4.17 | 3.87 | 7.89 | 6.73 |
| **4** | 1HN | 4.57 | 4.28 | 4.03 | 3.80 | 7.94 | 7.30 |
| **5** | 2HN | 4.38 | 4.34 | 4.01 | 3.70 | 7.81 | 7.38 |
| **6** | 23DMN | 4.53 | 4.28 | 4.16 | 3.86 | 7.85 | 6.69 |
| **7** | 26DMN | 4.52 | 4.36 | 4.19 | 3.80 | 7.76 | 7.07 |
| **8** | 2PN | 4.36 | 4.29 | 3.92 | 3.55 | 8.56 | 6.36 |
| **9** | 14DPN | 4.20 | 4.12 | 3.37 | 3.26 | 8.66 | 8.33 |
| **10** | 15DPN | 4.28 | 4.10 | 3.50 | 3.31 | 8.56 | 8.48 |
| **11** | 17DPN | 4.20 | 4.17 | 3.42 | 3.40 | 8.38 | 7.18 |
| **12** | ACN | 4.58 | 4.30 | 4.13 | 3.86 | 8.10 | 7.29 |
| $\langle \Delta_X \rangle^{b,c}$ | | 0.19 | | 0.27 | | 0.98 | |
| $\langle \lvert \Delta_X \rvert \rangle^{b,d}$ | | 0.19 | | 0.27 | | 0.98 | |

[a] Experimental values from Berlman *et al.*[S1]
[b] $\Delta_X = X_{\mathrm{theory}} - X_{\mathrm{expt}}$. $X = E_{\mathrm{abs}}$, $E_{\mathrm{fl}}$ or $k_{\mathrm{fl}}$.
[c] Mean signed error (MSE).
[d] Mean absolute error (MAE).
[f] Kasha emission $S_1 \rightarrow S_0$.

**Table S2: $E_{\mathrm{abs}}$'s, $E_{\mathrm{fl}}$'s and $k_{\mathrm{fl}}$'s for Family II from theory and experiments.**

| | | $E_{\mathrm{abs}}$ (eV) | | $E_{\mathrm{fl}}$ (eV) | | $\log_{10}(k_{\mathrm{fl}}/\mathrm{s}^{-1})$ | |
|---|---|---|---|---|---|---|---|
| # | species | theory | expt | theory | expt | theory[g] | expt |
| **13** | 1AN[a] | 4.25 | 3.90 | 3.60 | 3.29 | 7.82 | 7.82 |
| **14** | 1A4CNN[a] | 4.18 | 3.72 | 3.74 | 3.22 | 8.17 | 8.15 |
| **15** | 1A4CLN[a] | 4.12 | 3.79 | 3.48 | 3.19 | 7.88 | 7.88 |
| **16** | 1A4MN[a] | 4.14 | 3.82 | 3.44 | 3.18 | 7.82 | 7.72 |
| **17** | 1MAN[a] | 4.14 | 3.72 | 3.52 | 3.23 | 7.87 | 7.80 |
| **18** | 1DMAN[b] | 4.18 | 4.07 | 3.54 | 3.22 | 7.97 | 7.93 |
| **19** | 1DMA4CNN[a] | 4.00 | 3.69 | 3.57[h] | 3.17 | 8.27[h] | 8.54 |
| **20** | 1DMA4CLN[a] | 4.06 | 3.89 | 3.44 | 3.14 | 8.03 | 8.03 |
| **21** | 1DMA4MN[a] | 4.11 | 3.96 | 3.42 | 3.14 | 7.95 | 7.92 |
| **22** | 1DMA4MON[b] | 4.06 | 3.77 | 3.23 | 3.01 | 7.82 | 7.90 |
| **23** | 1DMA5MON[b] | 4.28 | 4.08 | 3.73 | 3.35 | 8.22 | 7.90 |
| **24** | 1DMA6MON[b] | 4.11 | 4.09 | 3.50 | 3.22 | 7.95 | 7.86 |
| **25** | 1DMA7MON[b] | 4.04 | 4.22 | 3.42 | 3.15 | 7.92 | 7.70 |
| **26** | 1NAZN[c] | 4.15 | 3.80 | 3.55 | 3.17 | 7.99 | 7.89 |
| **27** | 1NPYN[c] | 4.06 | 3.90 | 3.54[h] | 3.21 | 8.01[h] | 7.94 |
| | $\langle\Delta_X\rangle$[d,e] | 0.23 | | 0.32 | | 0.05 | |
| | $\langle\lvert\Delta_X\rvert\rangle$[d,f] | 0.26 | | 0.32 | | 0.05 | |

[a] Experimental values from Suzuki *et al.*[S2]
[b] Experimental values from Takehira *et al.*[S3]
[c] Experimental values from Rückert *et al.*[S4]
[d] $\Delta_X = X_{\mathrm{theory}} - X_{\mathrm{expt}}$. $X = E_{\mathrm{abs}}$, $E_{\mathrm{fl}}$ or $k_{\mathrm{fl}}$.
[e] Mean signed error (MSE).
[f] Mean absolute error (MAE).
[g] Kasha emission $S_1 \rightarrow S_0$.
[h] Evaluated at an $S_1$ geometry optimized using a range-separated varient of PBE with 50% Hartree–Fock exchange in the short-range and $\omega = 0.2$ bohr$^{-1}$ as the species collapsing into an unphysical charge-transfer excited state.

**Table S3: Experimental $k_{\mathrm{nr}}$'s are compared against theoretical direct $k_{\mathrm{ISC}}$'s for Family I. Theoretical values of $E_{\mathrm{ISC}}$'s, $\lambda_{\mathrm{ISC}}$'s, and $E^{\ddagger}_{\mathrm{ISC}}$'s are also provided.**

| # | Species | $\log_{10}(k_{\mathrm{nr}}/\mathrm{s}^{-1})^a$ expt$^a$ | $\log_{10}(k_{\mathrm{ISC}}/\mathrm{s}^{-1})^b$ theory | $E_{\mathrm{ISC}}$ theory | $\lambda_{\mathrm{ISC}}$ theory | $E^{\ddagger}_{\mathrm{ISC}}$ theory |
|---|---|---|---|---|---|---|
| **1** | NAPH | 6.90 | 6.92 | 1.41 | 0.26 | 2.71 |
| **2** | 1MN | 7.05 | 7.08 | 1.36 | 0.25 | 2.58 |
| **3** | 2MN | 7.06 | 7.36 | 1.39 | 0.26 | 2.63 |
| **4** | 1HN | 7.87 | 7.43 | 1.26 | 0.25 | 2.30 |
| **5** | 2HN | 7.71 | 7.86 | 1.29 | 0.26 | 2.32 |
| **6** | 23DMN | 6.90 | 7.65 | 1.37 | 0.25 | 2.60 |
| **7** | 26DMN | 7.16 | 7.62 | 1.35 | 0.24 | 2.63 |
| **8** | 2PN | 6.81 | 7.12 | 1.17 | 0.29 | 1.83 |
| **9** | 14DPN | 8.51 | 7.96 | 1.00 | 0.30 | 1.41 |
| **10** | 15DPN | 8.42 | 7.74 | 1.02 | 0.25 | 1.61 |
| **11** | 17DPN | 7.23 | 7.07 | 0.98 | 0.26 | 1.46 |
| **12** | CAN | 7.12 | 6.92 | 1.31 | 0.25 | 2.42 |

[a] Experimental $k_{\mathrm{ISC}}$ values obtained from Berlman *et al.*[S1]
[b] Predicted $k_{\mathrm{ISC}}$ values in this work using Eq. (5) in the main text with $B = 8.32 \times 10^6$ s$^{-1}$ and $C = 1.66 \times 10^7$ s$^{-1}$ cm$^2$, respectively.

**Table S4: Experimental $k_{\mathrm{nr}}$'s are compared against theoretical direct $k_{\mathrm{IC}}$'s for Family II. Theoretical values of $E_{\mathrm{fl}}$'s, $\lambda_{\mathrm{IC}}$'s, and $E^{\ddagger}_{\mathrm{IC}}$'s are also provided.**

| # | Species | $\log_{10}(k_{\mathrm{IC}}/\mathrm{s}^{-1})^{a,b,c}$ expt | $\log_{10}(k_{\mathrm{IC}}/\mathrm{s}^{-1})^{d}$ theory | ${E_{\mathrm{IC}}}^{e}$ theory | $\lambda_{\mathrm{IC}}$ theory | $E^{\ddagger}_{\mathrm{IC}}$ theory |
|---|---|---|---|---|---|---|
| **13** | 1AN[a] | 7.92 | 7.39 | 3.61 | 0.37 | 10.80 |
| **14** | 1A4CNN[a] | 9.21 | 9.07 | 3.46 | 0.26 | 13.20 |
| **15** | 1A4CLN[a] | 8.25 | 7.54 | 3.47 | 0.36 | 10.21 |
| **16** | 1A4MN[a] | 7.49 | 6.52 | 3.49 | 0.38 | 9.81 |
| **17** | 1MAN[a] | 7.66 | 7.76 | 3.55 | 0.35 | 10.87 |
| **18** | 1DMAN[b] | 9.93 | 9.13 | 3.59 | 0.40 | 9.97 |
| **19** | 1DMA4CNN[a] | 11.24 | 10.92 | 3.34 | 0.29 | 11.31 |
| **20** | 1DMA4CLN[a] | 10.24 | 9.39 | 3.46 | 0.39 | 9.53 |
| **21** | 1DMA4MN[a] | 9.36 | 8.73 | 3.51 | 0.42 | 9.24 |
| **22** | 1DMA4MON[b] | 8.45 | 8.36 | 3.44 | 0.46 | 8.34 |
| **23** | 1DMA5MON[b] | 9.85 | 9.31 | 3.66 | 0.34 | 11.85 |
| **24** | 1DMA6MON[b] | 9.85 | 8.26 | 3.49 | 0.37 | 10.16 |
| **25** | 1DMA7MON[b] | 7.91 | - | 3.45 | 0.37 | 9.84 |
| **26** | 1NAZN[c] | 8.68 | 9.72 | 3.52 | 0.36 | 10.56 |
| **27** | 1NPYN[c] | 10.09 | 11.29 | 3.50 | 0.32 | 11.52 |

[a] Experimental values from Suzuki *et al.*[S2]
[b] Experimental values from Takehira *et al.*[S3]
[c] Experimental values from Rückert *et al.*[S4]
[d] Predicted $k_{\mathrm{IC}}$ values in this work using Eq. (5) in the main text with $A_{\mathrm{IC}} = 2.02 \times 10^{12}$ s$^{-1}$ and the slope of $-8.18$ eV$^{-1}$.

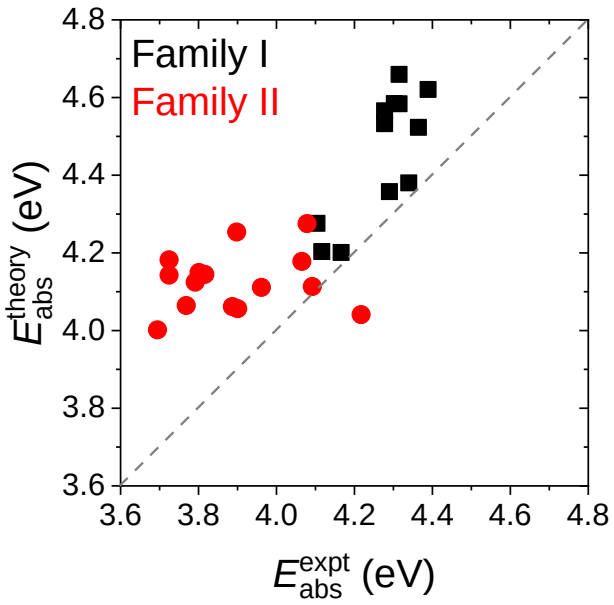


Figure S1: Comparison between the theoretical and experimental values for $E_{\text{abs}}$ for Families I (black squares) and II (red circles).

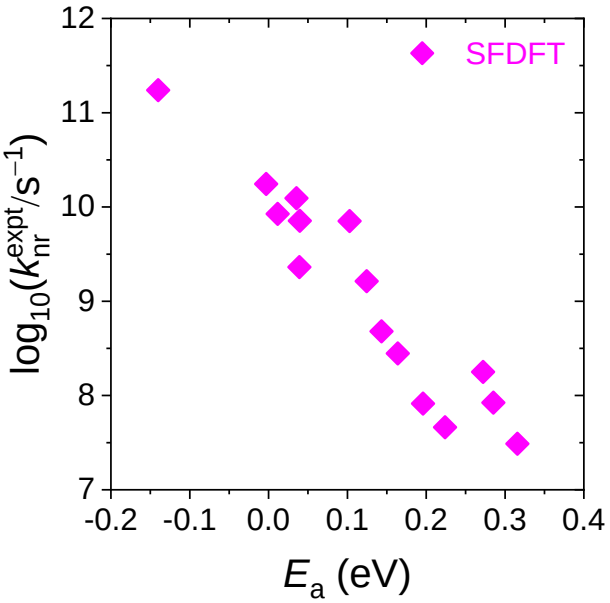


Figure S2: Energy gap law correlations between $k_{nr}$ and the $E_a$ evaluated using the SFDFT/BHHLYP approach. $E_a$ is treated as the difference between the FC minimum on the $S_1$ surface and the $S_1/S_0$ MECI.

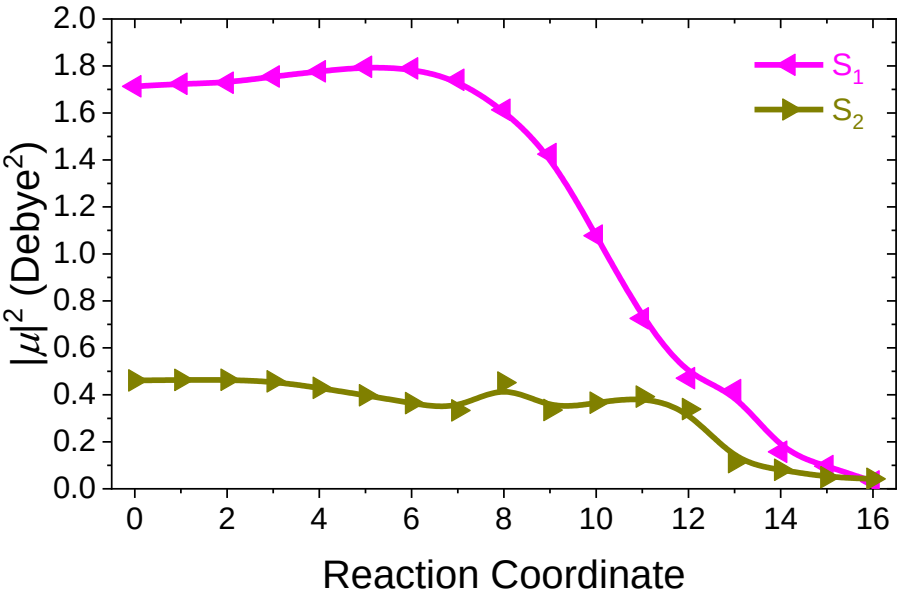


Figure S3: The squared TDMs for the $S_0 \rightarrow S_1$ and $S_0 \rightarrow S_2$ transitions along the reaction path described in Fig. 6 of the main text. $S_1$ and $S_2$ do not seem to switch in character.

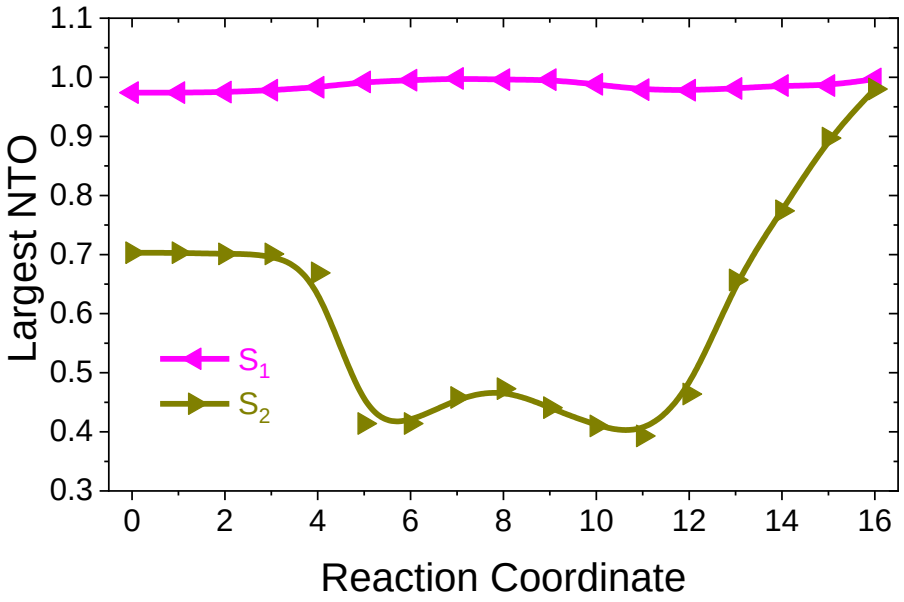


Figure S4: The percentage of the largest NTOs of the $S_0 \rightarrow S_1$ and $S_0 \rightarrow S_2$ transitions along the reaction path described in Fig. 6 of the main text. $S_1$ and $S_2$ do not seem to switch in character.

# References


(S1) Berlman, I. B. In *Handbook of Fluorescence Spectra of Aromatic Molecules*, 2nd ed.; Berlman, I. B., Ed.; Academic Press, 1971; pp 107–415.

(S2) Suzuki, K.; Demeter, A.; Kühnle, W.; Tauer, E.; Zachariasse, K. A.; Tobita, S.; Shizuka, H. Internal conversion in 4-substituted 1-naphthylamines. Influence of the electron donor/acceptor substituent character. *Phys. Chem. Chem. Phys.* **2000**, *2*, 981–991.

(S3) Takehira, K.; Suzuki, K.; Hiratsuka, H.; Tobita, S. Fast internal conversion in 1-(dimethylamino)naphthalene: Effects of methoxy substitution on the naphthalene ring. *Chem. Phys. Lett.* **2005**, *413*, 52–58.

(S4) Rückert, I.; Demeter, A.; Morawski, O.; Kühnle, W.; Tauer, E.; Zachariasse, K. A. Internal conversion in 1-aminonaphthalenes. Influence of amino twist angle. *J. Phys. Chem. A* **1999**, *103*, 1958–1966.